25th ABCM International Congress of Mechanical Engineering
October 20-25, 2019, Uberlândia, MG, Brazil

COB-2019-0963
NUMERICAL STUDY OF RUGOSITY EFFECTS IN A SINUSOIDAL PIPE BY APPLYING K-OMEGA SST TURBULENCE MODEL

Paulo Gabriel Cunha Martins
Kesiany Máxima de Souza
Marcelo José Santos de Lemos
Instituto Tecnológico de Aeronáutica, Aeronautic and Mechanical Department, São José dos Campos, Brasil
paulomartins92@gmail.com
kesianymaxima@gmail.com
delemos@ita.br

Abstract. *Corrugated walls are widely applied in industry to increase the heat transfer between the inner flow and the outer environment. The present study aims to analyze the flow properties inside a corrugated pipe considering different levels of wall roughness. The k-ω SST turbulence model was chosen since it deals with flow detachment near the wall and recirculation bubble with good accuracy at low computational cost. The approach method was validated by comparing the friction factors in a straight pipe with literature results. After a grid independence study, the corrugated pipe simulation allowed important observations such as the drop of the velocity in center-line, an increase of the head loss, a slow diminishing of the vortices, and an increase of the shear stress on the throats all caused by an intensification of the wall roughness.*

Keywords: *Corrugated Pipe, Turbulent Modeling, Roughness, k-ω SST turbulence model*

1. INTRODUCTION

As cited by Habib *et al.* (1998), efforts have been made in search of more efficient and compact heat transfer surfaces, which have allowed important advances in several fields such as spacecraft, air conditioning, aircraft, medicine, etc. As an example, the corrugate pipe offers high efficiency and allows the application of shorter pipes when compared to straight ones.

In aerospace industry, besides the direct application of sinusoidal surfaces in heat exchanges, the importance of corrugated pipes is also that it allows the study of viscous fluid flow pasts a wavy boundary, which can be observed in transpiration cooling of re-entry vehicles and rocket boosters, film vaporization in combustion chambers, cross-hatching on ablative surfaces and possibly drag reduction (Habib *et al.*, 1998).

Kasim *et al.* (2017) has researched advanced heat transfer devices for aerospace applications that are being developed to meet the aerospace need for efficient thermal performance with low weight, volume, and parasitic penalties. Plain, offset, wavy and louvered fin types have been widely applied in aerospace heat exchanges since they can offer great thermal-hydraulic performance, low cost, and high adjustability.

Thus, the use of convergent-divergent or corrugated channels is widely used to optimize heat transfer, as also cited by Habib *et al.* (1998), Pehlivan (2013), and Wang and Chen (2002). So, to better understand the behavior of a fluid flowing in a wave surface, the objective of the present work is to analyze the fluid dynamics in a wave pipe and the effects of roughness on the main properties of the flow. Wall roughness effects in heat transfer and head loss inside straight pipes have been vastly researched in literature, but the relation of head loss and relative roughness in corrugated pipes have not yet been assessed. This work aims the study of water flow properties inside a pipe with a corrugated wall to observe the variation of these properties, such as velocity, pressure and shear stress, with the increase of wall roughness.

To perform the numerical study, the software ANSYS Fluent was used to simulate the water flow in the turbulent regime within the sinusoidal pipe. A study of the turbulence model and grid independence was performed to analyze the flow properties in a section that the flow was fully developed considering different levels of roughness on the wall.

Initially, the k-ϵ model (Jones, W P; Launder, 1972) was considered for this case due to its robustness, but the presence of fluid detachment near the wall and the recirculating zone interfered in the quality of the results and then, this model was discarded. With that, the k-ω SST model (Menter, 1994) was applied, since it is a low Reynolds model and has two functions: near the wall it calculates the properties of the fluid more precisely using the standard k-ω model from Wilcox (1993), and in the core of the fluid it uses the k-ϵ model, which results in the best performance of both models.

A tube of a constant cross-section with different roughness levels on the wall was simulated to validate the numerical methods employed. Then, the results of the friction factors were compared with those obtained experimentally by Colebrook (1939), Haaland (1983), and Swamee and Jain (1976). After validation of the methods, a grid independence study for the corrugated pipe simulation was performed to assure the quality of the results.

Finally, as the main objective of this work, a section of the corrugated pipe with fully developed turbulent flow considering different roughness levels on the wall could be analyzed. The results of velocity and head loss profiles in the center-line of the pipe, shear stresses and friction factors on the wall were then obtained and discussed.

2. TURBULENT NUMERICAL METHOD

A turbulent flow of water through a corrugated tube with 16 sections was simulated at Ansys Fluent. Initially, the 2 equations standard k-ϵ model (Jones, W P; Launder, 1972) was tested, but it did not perform satisfactorily in the present study because it is a high Reynolds model and does not perform well close to the wall, requiring a wall function that is within the region $30 \leq y^+ \leq 300$. Since the mesh was very coarse with the standard wall function model, the scalable wall functions were used to have freedom in the refinement of the mesh. However, the results presented inconsistencies in cases with greater roughness on the wall. In conclusion, this model is not suitable for cases with a detachment of the fluid near the wall or in the presence of recirculation zones, which is one of the reasons that led to the creation of the k-ω model by Wilcox (1993).

Therefore, the turbulence model chosen is the k-ω SST developed by Menter (1994), due to its hybrid function of using the low Reynolds standard k-ω model from Wilcox (1993), and also a transformed k-ϵ model from Jones, W P; Launder (1972) towards the boundary layer via a blending function.

2.1 Mean flow equations

The k-ω SST model uses the $RANS$ (Reynolds-Averaged Navier-Stokes) equations, therefore the solution is decomposed into the mean (time-averaged or ensemble-averaged) and the fluctuating components Ansys (2006b). Consider velocity, pressure or any scalar quantity represented by ϕ_i, it can be decomposed as shown in Eq. (1) into a mean $\bar{\phi_i}$ and a fluctuating value ϕ_i'.

$$\phi_i = \bar{\phi_i} + \phi_i' \tag{1}$$

Writing in cartesian tensor form, discarding the time factor of the equations (steady-state simulation) and dropping the overbar on the mean velocity, the equations for the mass and momentum conservation, Eqs. (2) and (3), respectively, yields to the ensemble-averaged mass and momentum equations (Ansys, 2006b). Where ρ is the fluid density, u is the fluid velocity, p is pressure, and μ is the fluid molecular viscosity. Those equations are the well-known $RANS$ equations, which have the same format as the Navier-Stokes equations, but the velocity, pressure and other variables are in ensemble-averaged format.

$$\frac{\partial(\rho u_i)}{\partial x_i} = 0 \tag{2}$$

$$\frac{\partial(\rho u_i u_j)}{\partial x_j} = \frac{\partial p}{\partial x_i} + \frac{\partial}{\partial x_j}\left[\mu\left(\frac{\partial u_i}{\partial x_j} + \frac{\partial u_j}{\partial x_i} - \frac{2}{3}\delta_{ij}\frac{\partial u_l}{\partial x_l}\right)\right] + \frac{\partial}{\partial x_j}\left(-\rho\overline{u_i' u_j'}\right) \tag{3}$$

2.2 Transport equations

The Reynolds stresses are closed via the Boussinesq hypothesis by been modeled using an eddy (or turbulent) viscosity μ_T (Ansys, 2006a), as shown in Eq. (4), where k is the turbulent kinetic energy, and τ is the shear stress. Observe that, for incompressible flow, $\partial\bar{u_k}/\partial x_k = 0$.

$$-\rho\overline{u_i' u_j'} = \mu_T\left(\frac{\partial\bar{u_i}}{\partial x_j} + \frac{\partial\bar{u_j}}{\partial x_i}\right) - \frac{2}{3}\mu_T\frac{\partial\bar{u_k}}{\partial x_k}\delta_{ij} - \frac{2}{3}\rho k\delta_{ij} \;=\; \tau_{ij} \tag{4}$$

The eddy viscosity in the $k-\omega$ SST model is a function of the turbulent kinetic energy k and the specific turbulent dissipation rate ω, as presented in Eq. (5).

$$\mu_T = f\left(\frac{\rho k}{\omega}\right) \tag{5}$$

Where:

$$k = \frac{\overline{u_i' u_i'}}{2} \tag{6}$$

$$\varepsilon = \nu \ \overline{\frac{\partial u\prime_i}{\partial x_j}\left[\left(\frac{\partial u\prime_i}{\partial x_j} + \frac{\partial u\prime_j}{\partial x_i}\right)\right]} \tag{7}$$

$$\omega = \frac{\varepsilon}{k} \tag{8}$$

The fundamental idea of the $k-\omega\ SST$ model is the use of a blending function that unites the best of what the standard $k-\omega$ model and the $k-\epsilon$ model has to offer, this is done by the function presented in Eq. (9), where ϕ_1 is the original $k-\omega$ model that is multiplied to F_1 and ϕ_2 is the transformed $k-\epsilon$ turbulence model. The function F_1 is equal to one in the near-wall region and zero away from the surface.

$$\phi = F_1\phi_1 + (1-F_1)\phi_2 \tag{9}$$

The Shear Stress Transport model for the two-equations model computes τ as shown in Eq. (10) (Menter, 1994), where $\Omega = \partial u/\partial y$.

$$\tau = \mu_T\Omega = \rho\sqrt{\frac{Production_k}{Dissipation_k}}a_1 k \tag{10}$$

The SST model for the full Reynolds-stress models follows the Bradshaw's assumption that the shear stress in the boundary layer is proportional to the turbulent kinetic energy k. To satisfy this assumption for the eddy-viscosity model, the eddy viscosity was defined by Menter (1994) as shown in Eq. (11). Where F_2 is one for the boundary layers flow and zero for free shear layers.

$$\nu_T = \frac{a_1 k}{max(a_1\omega; \Omega F_2)} \tag{11}$$

The functions F_1 and F_2 are defined by Eqs. (12)-(16) (Menter, 1994):

$$F_1 = tanh(arg_1^4) \tag{12}$$

$$arg_1 = min\left(max\left(\frac{\sqrt{k}}{0.09\omega k}; \frac{500\mu}{\rho\omega y^2}\right); \frac{4\rho\sigma_{\omega 2}k}{CD_{k\omega}y^2}\right) \tag{13}$$

$$CD_{k\Omega} = max\left(2\rho\sigma_{\omega 2}\frac{1}{\omega}\frac{\partial k}{\partial x_j}\frac{\partial \omega}{\partial x_j}; 10^{-20}\right) \tag{14}$$

$$F_1 = tanh(arg_2^2) \tag{15}$$

$$arg_2 = max\left(2\frac{\sqrt{k}}{0.09\omega y}; \frac{500\nu}{y^2\omega}\right) \tag{16}$$

The SST model is represented by the following equations for k and ω, knowing that $D/D_t = \partial/\partial t + u_i\partial/\partial x_i$.

$$\frac{D(\rho k)}{Dt} = \tau_{ij}\frac{\partial u_i}{\partial x_j} - \beta^*\rho\omega k + \frac{\partial}{\partial x_j}\left[(\mu + \sigma_k\mu_t)\frac{\partial k}{\partial x_j}\right] \tag{17}$$

$$\frac{D(\rho\omega)}{Dt} = \frac{\gamma}{\nu_T}\tau_{ij}\frac{\partial u_i}{\partial x_j} - \beta\rho\omega^2 + \frac{\partial}{\partial x_j}\left[(\mu + \sigma_\omega\mu_t)\frac{\partial \omega}{\partial x_j}\right] + 2\rho(1-F_1)\sigma_{\omega 2}\frac{1}{\omega}\frac{\partial k}{\partial x_j}\frac{\partial \omega}{\partial x_j} \tag{18}$$

The constants for the $k-\omega\ SST$ are the following:
$\sigma_{k1} = 0.85$; $\sigma_{\omega 1} = 0.5$;$\beta_1 = 0.075$; $a_1 = 0.31$; $\beta^* = 0.09$; $\gamma_1 = \beta_1/\beta^* - \sigma_{\omega 1}\kappa^2/\sqrt{\beta^*}$
$\sigma_{k2} = 1$; $\sigma_{\omega 2} = 0.856$; $\beta_2 = 0.0828$; $\gamma_2 = \beta_2/\beta^* - \sigma_{\omega 2}\kappa^2/\sqrt{\beta^*}$
where κ is the Von Kármán constant (0.41).

2.3 Near wall treatment

The turbulence model $k-\omega\ SST$ is quite precise and robust in the regions near the wall, it can adequately detail the boundary layer when its mesh requirements are established, among them $y^+ \simeq 1$ and enough nodal points (> 10) within the buffer region and sub-layers. This level of refinement ($y^+ \simeq 1$) turns the simulation extremely expensive for the industry because, beyond the higher quantity of cells elements throughout the wall region and depending on the geometry

- with curved edges for example -, it may be difficult to obtain a structured grid all over the control volume, turning the simulation quite heavy. On the other hand, the use of wall functions, which allows the use of coarser grids, limits the precision of the results when a more refined mesh is used.

Thanks to the work of Esch and Menter (2003), in the current software (ANSYS Fluent, CFX) the $k-\omega\ SST$ turbulence model uses a hybrid function that uses or not the wall functions depending on the value of y^+. In locations where $y^+ > 1$, the wall functions are automatically activated, thus allowing the use of this turbulence model with a less refined mesh without losing the quality of the results, as can be observed in the paper of Menter *et al.* (2003).

Following, it is shown how ANSYS Fluent performs the treatment on the wall and how the hybrid function is considered, as explained in Ansys (2006c). The value of ω close to the wall is calculated as shown in Eq. (19).

$$\omega_\omega = \frac{\rho(u^*)^2}{\mu}\omega^+ \tag{19}$$

The value of ω^+ is calculated according to the value of y^+. If the mesh is sufficiently refined ($y^+ \leq 1$) then ω^+ is calculated in the laminar sub-layer as shown in Eq. (20), where ω_ω^+ is related to the value of k_s^+, which is defined in Eq. (21). So, for $k_s^+ < 25$, Eq. (22) defines ω_ω^+ , and for $k_s^+ \geq 25$, Eq. (23) defines ω_ω^+.

$$\omega^+ = min\left(\omega_\omega^+, \frac{6}{\beta_i(y^+)^2}\right) \tag{20}$$

$$k_s^+ = max\left(1.0, \frac{\rho k_s u^*}{\mu}\right) \tag{21}$$

$$\omega_\omega^+ = \left(\frac{50}{k_s^+}\right)^2 \tag{22}$$

$$\omega_\omega^+ = \frac{100}{k_s^+} \tag{23}$$

For higher values of y^+, ω^+ is calculated in the logarithmic region using the approximation of the wall function as shown in Eq. (24). Resulting, therefore, in a ω of the element next to the wall defined as shown in Eq. (25).

$$\omega^+ = \frac{1}{\sqrt{\beta_\infty^*}}\frac{du_{turb}^+}{dy^+} \tag{24}$$

$$\omega = \frac{u^+}{\sqrt{\beta_\infty^*}ky} \tag{25}$$

3. VALIDATION OF THE METHODS

To validate the turbulence model used, a 2D axis-symmetric simulation of a tube with a constant cross section was performed to compare the friction factor in the tube with Eqs. (26), (27) and (28), obtained experimentally by Swamee and Jain (1976), Colebrook (1939), and Haaland (1983), respectively. Where f stands for Darcy friction factor, e roughness of the pipe, D inlet diameter, and Re Reynolds number.

$$f = 0.25\left[log\left(\frac{e/D}{3.7} + \frac{5.74}{Re^{0.9}}\right)\right]^{-2} \tag{26}$$

$$\frac{1}{\sqrt{f}} = -2log\left(\frac{e/D}{3.7} + \frac{2.51}{Re\sqrt{f}}\right) \tag{27}$$

$$f = \frac{0.3086}{\left\{log\left[\frac{6.9}{Re} + \left(\frac{e/D}{3.7}\right)^{1.11}\right]\right\}^2} \tag{28}$$

The simulations were accomplished considering different roughness levels on the wall (e / D = 0, 1e-4, 1e-3, 5e-3, 1e-2, 2.5e-2 and 5e-2). The mesh used in this analysis is presented in Fig. 1 and it was refined up to the point of obtaining y^+ ranging from 1.25 to 1.46.

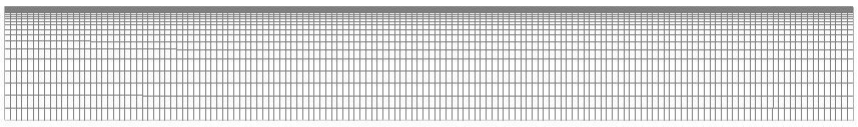

Figure 1. Mesh of the 2-D axis-symmetric pipe.

To verify the values of friction factors, it is necessary to guarantee that the section analyzed is fully developed. To do that, the velocity and head loss profile in the centerline of the straight pipe was assessed and as presented in Fig. 2.

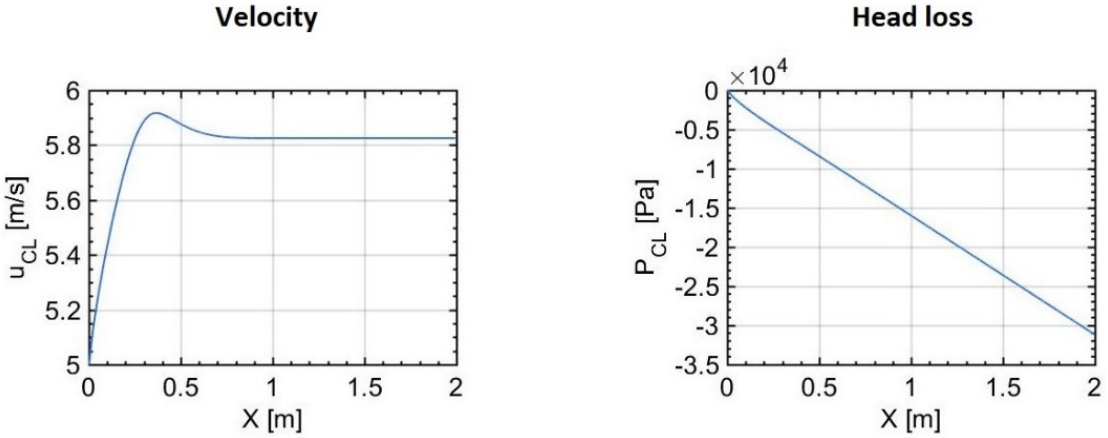

Figure 2. Velocity and pressure profiles along the centerline of the flow in the straight pipe.

Therefore, it is verified in Fig. 2 that the complete flow development is reached from 90 cm of the inlet, with that, the analysis of the friction factor was considered between 1.5 and 2 meters of the straight pipe. Moreover, the results are in good agreement with results from Joshi *et al.* (2014), where it is presented the overshooting of the velocity profile right before the full development of the flow. Therefore, the values of friction factors in the tube using the k-ω SST and k-ϵ turbulence models were analyzed and compared with results from Eqs. (26)-(28), as presented in Fig. 3.

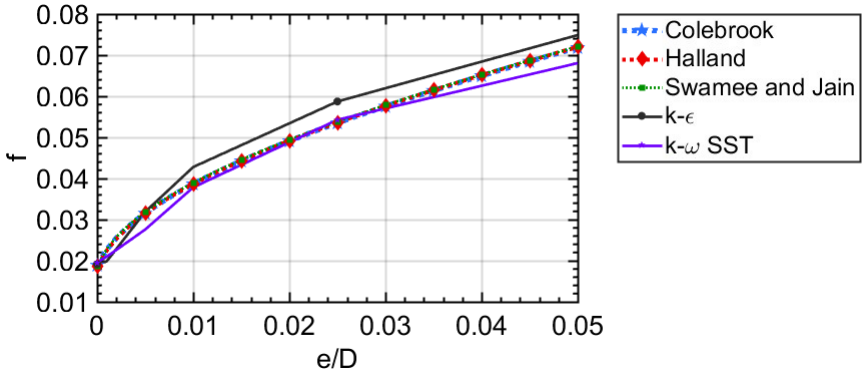

Figure 3. Results of the simulations compared to experimental Eqs. (26)-(28).

All three experimental results for the friction factors practically overlap. Moreover, the two simulations converged well to the experimental result for the smooth tube, diverging slightly in the rough tubes. The equations k-ϵ overestimates the friction factor values from e/D = 0.005 and the equations k-ω SST closely approximates the results between e/D = 0.01 and e/D = 0.025, but it slightly underestimates the result for the roughest case analyzed (e/D = 0.05).

4. RESULTS OF CORRUGATED PIPE SIMULATIONS

The control volume and the boundary conditions applied in the present numerical study are shown in Fig. 4 (A) and (B), respectively. The wall has a sinusoidal shape, in which D = 16 mm, H = 24 mm and L = 25.12 mm. This control surface admits an inlet velocity of water at 5 m/s, resulting in turbulent flow with Re = 80000.

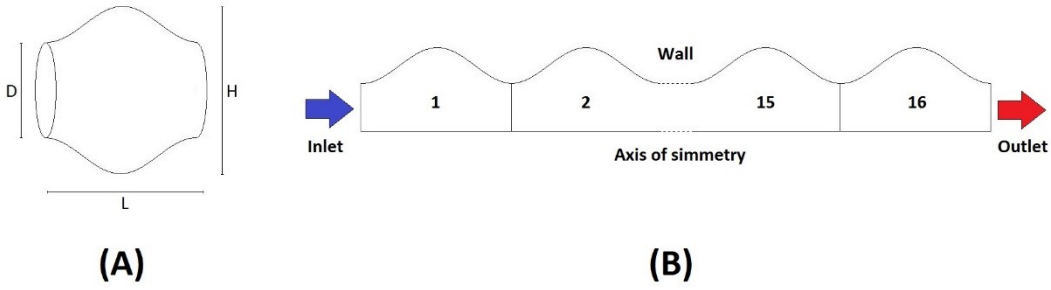

Figure 4. (A) Control volume of a unity section, and (B) boundary conditions from the simulation.

The structured mesh considered has 7766 elements per section as shown in Fig. 5, resulting in a total of 124256 elements in the domain. As calculated by Fluent, 40% of the elements in this mesh has a minimum orthogonality quality, and the grid has a maximum aspect ratio of 126.

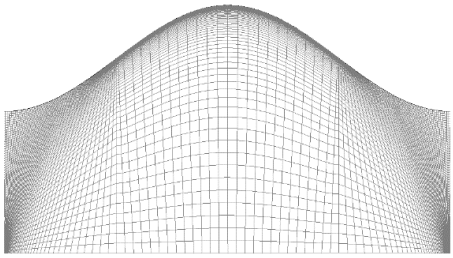

Figure 5. Mesh considered over one section.

As seen in previous relationships of near-wall treatment, ω is directly related to wall roughness. It was observed that ω increases proportionally with the relative roughness, which also happens for the y^+ as presented in Tab. 1.

Table 1. Distance from the first cell to the wall at all simulations.

$k-\omega\ SST$							
e/D	0	0.0001	0.001	0.005	0.01	0.025	0.05
y^+	2.42	3.04	3.46	8.38	15.32	37.33	77.04

Concerning the $k-\omega\ SST$ turbulence model and its mesh requirements, as mentioned previously, there is no problem to get y^+ values far from the unit due to the capacity of the model to predict this distance and to use a wall function in the logarithmic region. Thus, as seen in the work presented by Menter *et al.* (2003), it is expected errors lower or equal to 2%. To verify the grid independence, two other meshes were created, one more refined with 9348 elements per section and a second mesh with 7011 elements per section. With those meshes, simulations were performed considering all the roughness presented in Table 1, and from those simulations, the values of the friction factors of this corrugated tube were calculated using Eq. (29). The results are presented in Fig.6.

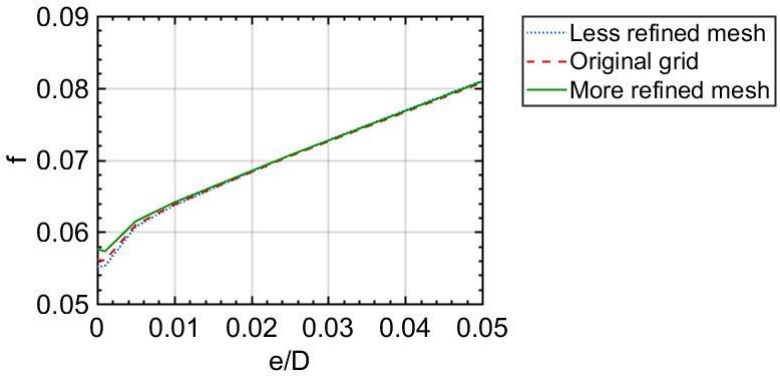

Figure 6. Friction factor calculated using 3 different meshes

$$f = \frac{\Delta P}{\frac{L}{D}\rho\frac{\nu^2}{2}} \tag{29}$$

For the smooth pipe, a maximum error of 2.7% was found between the most refined and the original mesh. Already for the rough wall simulations, the results are more alike with each other. A more refined mesh provides more reliable results but turns the simulation more expensive. Because the magnitude of the error was considered acceptable, the original mesh with 124256 elements was considered.

To verify whether the turbulent fluid was fully developed, the velocity and pressure profiles for the simulation of the corrugated pipe were investigated, and the results are presented in Fig. 7.

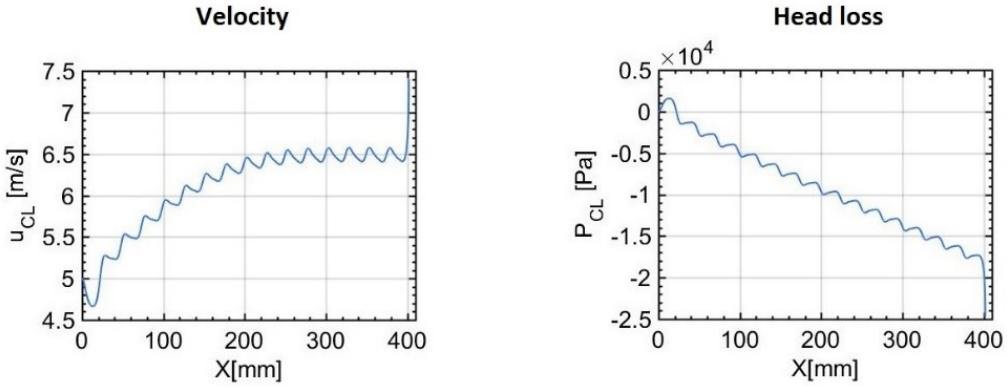

Figure 7. Velocity and pressure profile along the centerline of the flow for the corrugated pipe.

The most notable characteristic of the profiles shown in Fig. 7 is the wave behavior of the properties due to the geometry of the sinusoidal tube. Also, despite this behavior, a constant slope of the head loss can be verified after its transient region at the entrance. From the velocity plot in Fig. 7, it was found that the flow develops completely from the 11th section of the pipe. Comparing Fig. 2 and 7, a very important feature can be observed in the use of corrugated tubes rather than cylindrical tubes: the flow in corrugated tubes develops more quickly, more precisely, it took 30 cm to develop, while in the cylindrical tube, the fluid is fully developed from 90 cm.

In the last section of Fig. 7 the properties diverge somewhat, however the same does not happen for the straight pipe in Fig. 2. Since the same methodology for both simulations were applied, it was concluded that this is a numerical error and the 16th section of Fig. 7 should be disregarded from the analysis.

Therefore, the 15th section was chosen to be analyzed in this work. The velocity and head loss profiles were assessed in the central line of the flow. For the characterization of the recirculation zone, the shear stress was examined. As proof of complete fluid development, for all simulations, the velocities in the inlet and outlet throats of the 15th section were verified to be the same, as can be seen in Fig. 8.

Streamlines in the 15th section are shown in Fig. 9 for most of the cases analyzed. In this figure, the higher value of velocity is presented in the core of the flow and it decreases a little bit along with the size of the recirculation bubble and the increasing roughness.

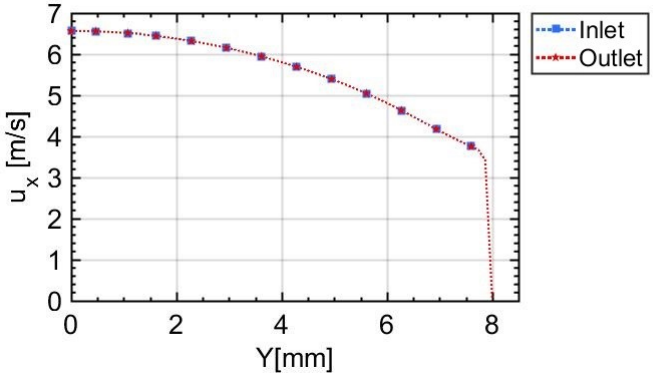

Figure 8. Velocity profile along the throat cross sections in the 15th section

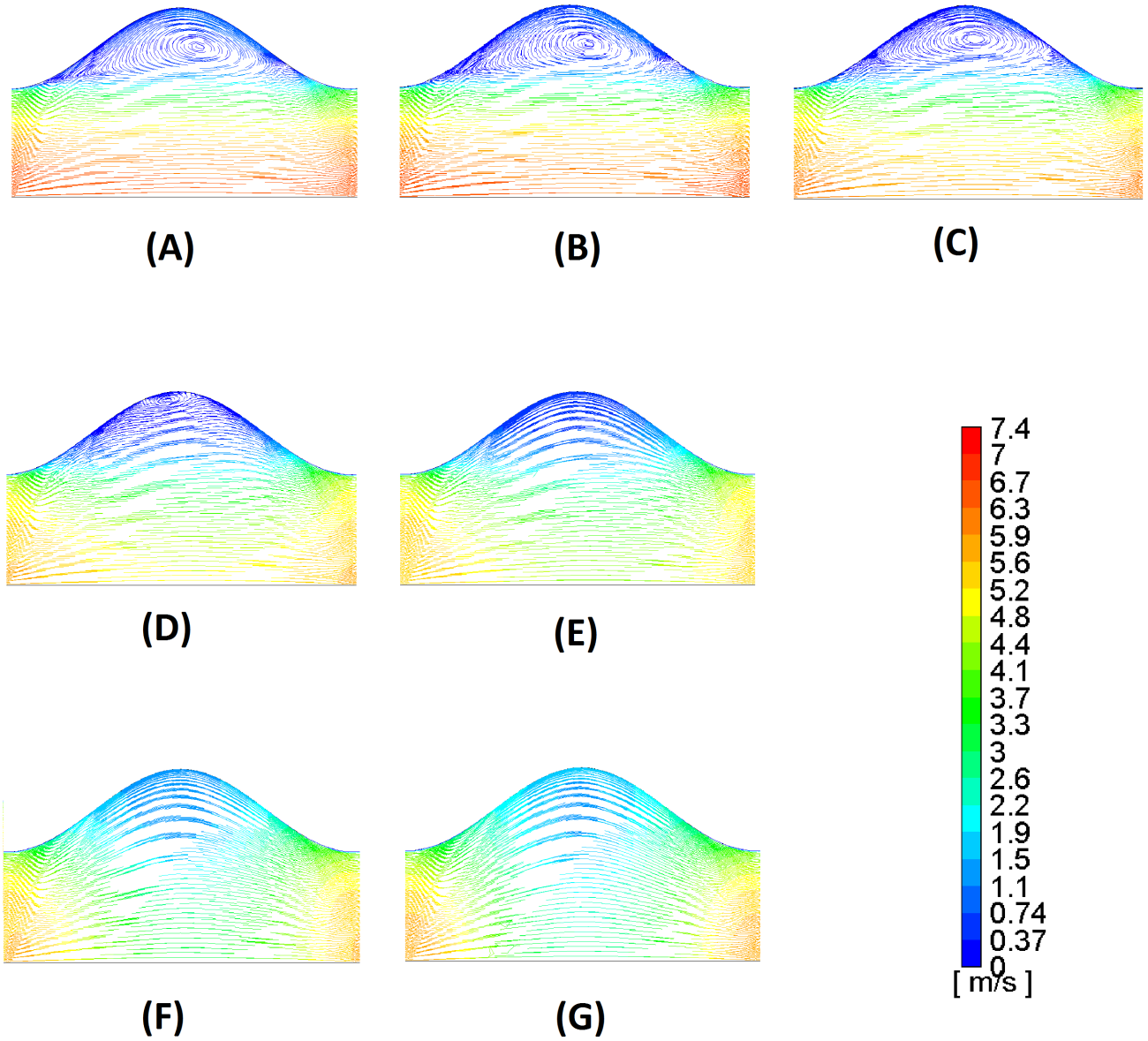

Figure 9. Velocity streamlines from the cases (A) smooth wall and rough wall with (B) e/D = 1e-4, (C) e/D = 1e-3, (D) e/D = 5e-3, (E) e/D = 1e-2, (F) e/D = 2.5e-2 and (G) e/D = 5e-2.

In the 15^{th} section of the sinusoidal tube, the velocity profile and the dimensionless head loss in the central line of the flow were analyzed. By making the local head loss dimensionless and considering the entry of the 15^{th} section as the

reference parameter in the analysis, the relation presented in Eq. (30) was investigated as shown in Fig. 10 (A), where $P_{x,CL}$ corresponds to the pressure at the centerline of the 15^{th} section in x position, f_x is the Darcy friction factor in x position, u_{inlet} is the flow inlet velocity, L is the section length, and D the inlet diameter.

$$f_x \frac{L}{D} = \frac{P_{x,CL} - P_{inlet,CL}}{\rho \frac{u_i nlet^2}{2}} \tag{30}$$

In Fig. 10 (A), the localized head loss increases together with the roughness in the central region of the section as well as in the outlet. With this increased roughness and head loss in the central region of the section, a decrease in speed is expected as shown in Fig. 10 (B).

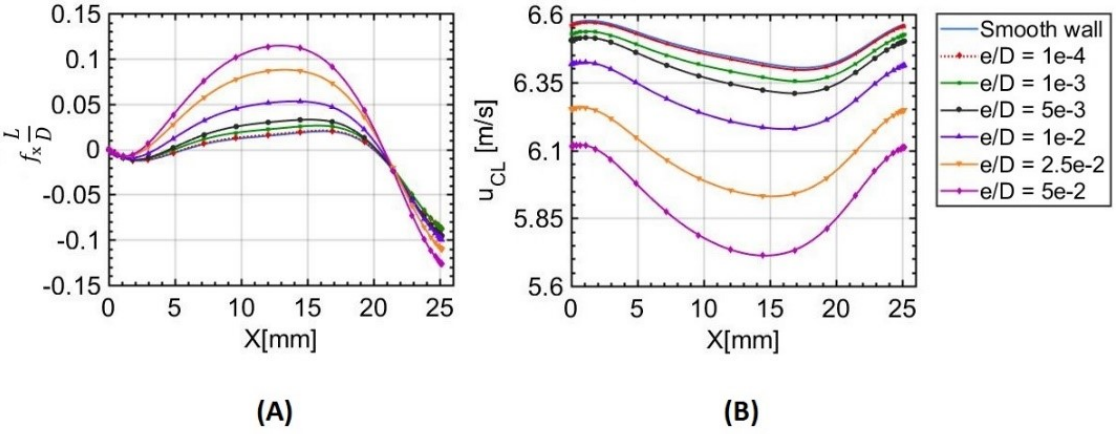

Figure 10. (A) Dimensionless localized head loss and (B) velocity profile in centerline from the 15^{th} section

Finally, it was evaluated the effect of the roughness variation on the vortex behavior. For that, the shear stress on the wall was investigated, and it was observed that when this value changes signal, the flow is in the region of the recirculating zone. In Fluent, by default, this value is mirrored in the x-axis, thus the position of the recirculating zone is allocated between the regions where the shear stress is zero as seen in Fig. 11.

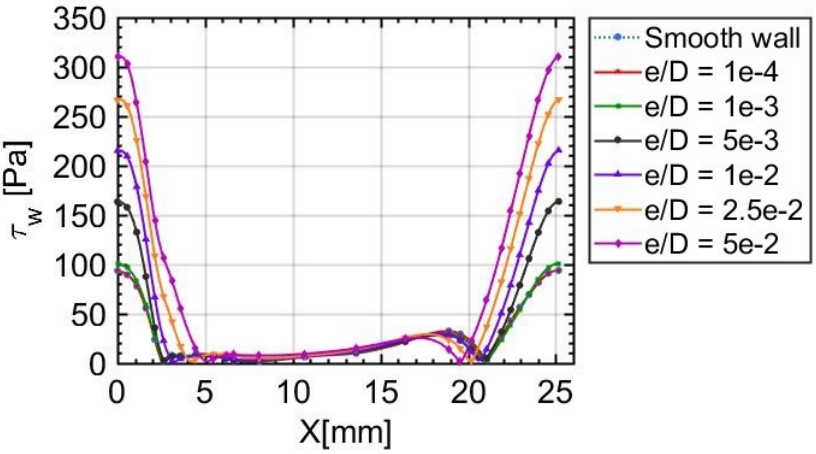

Figure 11. Absolute shear stress profile on the wall of the 15th section.

This recirculating zone becomes shorten with increasing roughness. In the smooth tube, we have a region comprising 18.42 mm in the x-direction, for the roughest case this value drops to 14.46 mm, that is, it decreased by 21.48% in that direction. Checking Fig. 9, it is noted that the vortex shrinks just a little bit with increasing roughness. Therefore, with the enlargement of roughness, there is a decrease in the central velocity of the flow, a diminishing of the vortex, an increase of the head loss, and an increase of the shear stress in the regions with smaller transversal areas, which will consequently contribute to the increase of heat transfer.

5. CONCLUSIONS

The numerical method was validated by comparing the values of friction factor in a straight pipe, at different roughness levels, with the experimental conjectures realized by Swamee and Jain (1976), Colebrook (1939), and Haaland (1983). With the validation of the methodology, it is believed that the results calculated for the corrugated pipe are reliable.

The results showed that an increase in the roughness of a corrugated pipe increases the head loss, decreases the minimum entrance length necessary for complete development of the fluid, slightly decreases the size of recirculating zones and increases the shear stress in regions of higher velocity - in the throats -, which also contributes to the overall increase in heat transfer, as seen in literature (Habib *et al.*, 1998), (Pehlivan, 2013), and (Wang and Chen, 2002). Therefore, the present study has reached a good agreement with the analytic and experimental results from literature.

6. ACKNOWLEDGEMENTS

The research was supported by the Coordination for the Improvement of Higher Education Personnel (CAPES), and National Council for Scientific and Technological Development (CNPq), Brazil.

7. REFERENCES

Ansys, 2006a. "Modeling turbulent flows". Introductory FLUENT Notes. 07 July 2018 <http://www.fluentusers.com>.

Ansys, 2006b. "Reynolds (ensemble) averaging". Fluent 6.3 User's Guide, section 12.2.2.

Ansys, 2006c. "Wall boundary conditions". Fluent 6.3 User's Guide, section 12.5.3.

Colebrook, C.F., 1939. "Turbulent flow in pipes, with particular reference to the transition region between the smooth and rough pipe laws." *Journal of the Institution of Civil Engineers*. ISSN 0368-2455. doi:10.1680/ijoti.1939.13150.

Esch, T. and Menter, F., 2003. "Heat transfer prediction based on two-equation turbulence models with advanced wall treatment". *Turbulence Heat an Mass Transfer 4*.

Haaland, S.E., 1983. "Simple and Explicit Formulas for the Friction Factor in Turbulent Pipe Flow". *Journal of Fluids Engineering*. ISSN 00982202. doi:10.1115/1.3240948.

Habib, M.A., Ul-Haq, I., Badr, H.M. and Said, S.A., 1998. "Calculation of turbulent flow and heat transfer in periodically converging-diverging channels". *Computers and Fluids*, Vol. 27, No. 1, pp. 95–120. ISSN 00457930. doi:10.1016/S0045-7930(97)00022-4.

Jones, W P; Launder, B.E., 1972. "The Prediction of Laminarization with a Two-Equation Model of Turbulence". *International Journal of Heat and Mass Transfer*, Vol. 15, pp. 301–314.

Joshi, M., Bisht, P. and Gupta, A., 2014. "Analysis of Fully Developed Turbulent Flow in a AXI-Symmetric Pipe using ANSYS FLUENT Software". *International Journal of Engineering Research and Technology*, Vol. 3, No. 3, pp. 723–728.

Kasim, K., Muley, A. and Stoia, M., 2017. "Advanced Heat Transfer Devices for Aerospace Applications". *Proceedings of the ASME 2017 International Mechanical Engineering Congress and Exposition*, pp. 1–7. doi:10.1115/IMECE2017-72382.

Menter, F.R., 1994. "Two-equation eddy-viscosity turbulence models for engineering applications". *AIAA Journal*, Vol. 32, No. 8, pp. 1598–1605. ISSN 0001-1452. doi:10.2514/3.12149.

Menter, F.R., Kuntz, M. and Langtry, R., 2003. "Ten Years of Industrial Experience with the SST Turbulence Model". *Turbulence Heat and Mass Transfer 4*, Vol. 4, pp. 625–632. ISSN 1662-8985. doi: 10.4028/www.scientific.net/AMR.576.60.

Pehlivan, H., 2013. "Experimental investigation of convection heat transfer in converging-diverging wall channels". *International Journal of Heat and Mass Transfer*. ISSN 00179310. doi:10.1016/j.ijheatmasstransfer.2013.06.033.

Swamee, P.K. and Jain, A.K., 1976. "Explicit equations for pipe-flow problems". *Journal of Hydraulic Division, ASCE*. ISSN 0044-796X.

Wang, C.C. and Chen, C.K., 2002. "Forced convection in a wavy-wall channel". *International Journal of Heat and Mass Transfer*. ISSN 00179310. doi:10.1016/S0017-9310(01)00335-0.

Wilcox, D., 1993. *Turbulence modeling for CFD*. ISBN 0963605100. doi:0963605151.